

Modeling of a membraneless single-chamber microbial fuel cell with molasses as an energy source

Bunpot Sirinutsomboon

Received: 15 December 2013 / Accepted: 17 March 2014
© The Author(s) 2014. This article is published with open access at Springerlink.com

Abstract Microbial fuel cell (MFC) is a novel bio-electrochemical system that can use various organic substances as energy source. Computational models of MFC are needed for prediction and optimization of the MFC performance. A comprehensive computational modeling of a membraneless single-chamber MFC, in which bacteria consumed molasses as a substrate, is reported here. The simulated cathode had a layer of polytetrafluoroethylene, which allowed oxygen molecules to diffuse through to take part in the reduction reaction. The substrate molecules diffused through the biofilm, which deposited on the anode surface, and were oxidized by the bacteria localized within the film. The simulation program accepted inputs such as the initial amount of molasses, thickness of the biofilm layer, and dimensions of the MFC chamber. Some outputs of the program include concentration profiles of molasses and oxygen as functions of time and location, and the open-circuit voltage of the MFC as a function of time. As the cathode thickness decreased or the biofilm increased, the voltage increased. To obtain a higher voltage, increasing the biofilm thickness was more effective than decreasing the cathode thickness when the initial COD levels were >5,000 mg/L.

Keywords Microbial fuel cell · Simulation · Molasses · Single chamber · Air cathode · Biofilm

Introduction

An electrochemical cell that employs bacteria as biocatalyst is called microbial fuel cell (MFC) [1]. An MFC can treat wastewater containing organic matters, which bacteria can consume, while simultaneously generating electricity. Molasses, as a by-product of cane sugar production process, has extensively been used to produce renewable energy such as ethanol and biogas. Wastewater from molasses-based distilleries can potentially be a substrate for MFCs [2].

Microbial fuel cells typically appear in two configurations: two chambers separated by a proton exchange membrane (PEM) or a single chamber. The focus here is in a membraneless single-chamber MFC [3]. The MFC has a cathode electrode with one side in contact with the liquid, while the other side is directly exposed to air. Oxygen in the air can passively diffuse through the cathode and involve in the reaction of oxygen reduction. This process requires no liquid aeration, which is energy intensive, thus saving cost and energy. A study [3] showed that the air-cathode MFC produced higher power output in the absence of PEM, which can obstruct the flow of protons. PEMs are also generally quite expensive. As a result, a membraneless single-chamber MFC is simple and inexpensive to build. Figure 1 shows a conceptual diagram of the MFC having molasses, of which primary sugar is sucrose ($C_{12}H_{22}O_{11}$) [4], as a main source of energy.

Computational simulation of an MFC requires a mathematical model that can predict the output and performance of the MFC. Knowledge in electrochemistry, reaction kinetics, and mass transport is required to derive the model. Various attempts to develop simulation models of biofilm on anode and two-chambered MFCs have been discussed [5–8]. The biofilm model only explained a portion of the

B. Sirinutsomboon (✉)
Department of Chemical Engineering, Faculty of Engineering,
Thammasat University, 99 Paholyotin Road, Klong-Luang,
Pathumthani 12120, Thailand
e-mail: bsirinut@engr.tu.ac.th

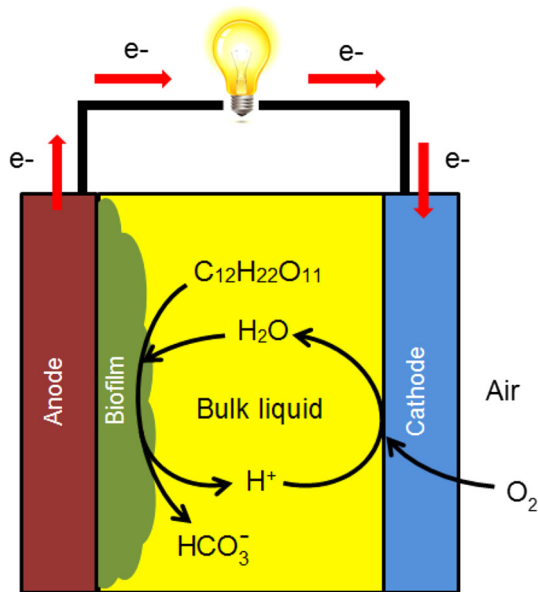


Fig. 1 A conceptual diagram of a membraneless single-chamber MFC

MFC process, while this paper presents a model describing the entire process of a single-chambered MFC. This type of modeling has never been reported in any literature. Here the results from a computational simulation based on the model are reported, in contribution to an ongoing study on the kinetic nature of the MFC process.

Methods

For the MFC simulation of interest, the cathodic reaction was the reduction of oxygen [1] as follows:



Sucrose was assumed to be the main substrate for the MFC, and made up about 50 % by weight of molasses [9]. With a similar stoichiometric approach as the oxidation of acetate [1], the equation for the oxidation of sucrose was derived. The anodic reaction is then given as follows:



The simulation was developed using Visual Basic program. The simulation program was mainly divided into two sequential segments; cathode and biofilm/anode. Each segment has a number of equations to be solved. The calculated outputs of the former segment were used by the latter.

Cathode

The cathode was assumed to have a layer of polytetrafluoroethylene (PTFE), which is permeable to oxygen but not water. The concentration profile of oxygen in the layer,

which was a function of both time and location, was calculated using Fick's second law of diffusion [10] as follows:

$$\frac{\partial}{\partial t} [\text{O}_2]_{\text{PTFE}} = D_{\text{O}_2, \text{PTFE}} \frac{\partial^2}{\partial y^2} [\text{O}_2]_{\text{PTFE}} \quad (3)$$

where

$[\text{O}_2]_{\text{PTFE}}$ concentration of oxygen in the PTFE layer, mmol dm^{-3}

$D_{\text{O}_2, \text{PTFE}}$ diffusivity of oxygen in PTFE, $\mu\text{m}^2 \text{min}^{-1}$

y location in the PTFE layer, μm

Presumably, only oxygen molecules that completely diffused through the PTFE layer and became dissolved in water could be reduced to yield water molecules. The reduction reaction thus occurred only at the cathode/liquid interface. The rate of oxygen reduction was speculated to follow the Monod equation and the Butler–Volmer equation [7, 11]. The two equations were thus combined into the following equation.

$$r_{\text{O}_2} = k_{\text{O}_2} \frac{[\text{O}_2]_{\text{cat/liq}}}{K_{\text{O}_2} + [\text{O}_2]_{\text{cat/liq}}} \exp \left[(1 - \alpha_{\text{cat}}) \gamma_{\text{e}^-/\text{O}_2} \frac{F}{RT} (E_{\text{cat}} - E_{\text{cat}}^o) \right] \quad (4)$$

where

r_{O_2} rate of oxygen reduction per area, $\text{mmol dm}^{-2} \text{min}^{-1}$

k_{O_2} rate constant of oxygen reduction per area, $\text{mmol dm}^{-2} \text{min}^{-1}$

$[\text{O}_2]_{\text{cat/liq}}$ concentration of oxygen at cathode/liquid interface, mmol dm^{-3}

K_{O_2} half velocity constant for oxygen, mmol dm^{-3}

α_{cat} electron-transfer coefficient of cathode

$\gamma_{\text{e}^-/\text{O}_2}$ electron equivalence of oxygen, $\text{mmol-electron mmol-oxygen}^{-1}$

F Faraday's constant, C mol^{-1}

R gas constant, $\text{J mol}^{-1} \text{K}^{-1}$

T temperature, K

E_{cat} cathode voltage, V

E_{cat}^o standard cathode voltage, V

The cathode voltage was calculated using the Nernst equation as follows [1]:

$$E_{\text{cat}} = E_{\text{cat}}^o - \frac{RT}{\gamma_{\text{e}^-/\text{O}_2} F} \ln \left(\frac{1}{[\text{O}_2]_{\text{cat/liq}} [\text{H}^+]_{\text{cat/liq}}^4} \right) \quad (5)$$

where

$[\text{O}_2]_{\text{cat/liq}}$ concentration of oxygen at cathode/liquid interface, mol dm^{-3}

$[\text{H}^+]_{\text{cat/liq}}$ concentration of hydrogen ion at cathode/liquid interface, mol dm^{-3}

Biofilm/anode

Sucrose was assumed to be the main substrate consumed by the bacteria, which were localized and dispersed throughout the biofilm. The biofilm was assumed to conduct electrons and considered to be part of the anode [5, 8, 11]. The rate of sucrose consumption was the same as the rate of exogenous respiration by the bacteria. The rate was described by the Nernst–Monod equation [5, 8] shown below. The active biomass referred to the live bacteria.

$$r_{\text{exo}} = \frac{\rho_b \mu_b X_b}{Y_b \gamma_{\text{COD/Suc}}} \cdot \frac{[\text{Suc}]_{\text{bio}}}{K_{\text{Suc}} + [\text{Suc}]_{\text{bio}}} \cdot \frac{1}{1 + \exp\left(-\frac{F}{RT} \eta\right)} \quad (6)$$

where

- r_{exo} rate of exogenous respiration in biofilm, $\text{mmol dm}^{-3} \text{ min}^{-1}$
- ρ_b density of active biomass, mg-VS dm^{-3} (VS, volatile solids, a measure of biomass)
- μ_b specific growth rate of active biomass, min^{-1}
- X_b volume fraction of active biomass (unitless) = $\frac{\text{volume of active biomass}}{\text{bulk volume}}$
- Y_b active biomass growth yield, mg-VS mg-COD^{-1}
- $\gamma_{\text{COD/Suc}}$ COD equivalence of sucrose, $\text{mg-COD mmol-sucrose}^{-1}$
- $[\text{Suc}]_{\text{bio}}$ concentration of sucrose in biofilm, mmol dm^{-3}
- K_{Suc} half velocity constant for sucrose, mmol dm^{-3}
- η local potential in biofilm, V

Along with the exogenous respiration, from which the bacteria obtained most energy, the endogenous respiration, by which the bacteria oxidized their own cellular mass, provided additional energy. The rate of endogenous respiration was described as follows [5, 8]:

$$r_{\text{endo}} = b_{\text{endo}} \rho_b X_b \frac{1}{1 + \exp\left(-\frac{F}{RT} \eta\right)} \quad (7)$$

where

- r_{endo} rate of endogenous respiration in biofilm, $\text{mg-VS dm}^{-3} \text{ min}^{-1}$
- b_{endo} endogenous decay coefficient of active biomass, min^{-1}

Based on the steady-state electron balance and Ohm’s law, the local potential, which was the driving force for electron movement in the biofilm, was calculated using the balance equation as follows [5, 8]:

$$\kappa_{\text{bio}} \frac{\partial^2 \eta}{\partial z^2} - \frac{F}{\tau \nu} \left(\gamma_{e^-/\text{Suc}} r_{\text{exo}} + \gamma_{e^-/b} r_{\text{endo}} \right) = 0 \quad (8)$$

where

- κ_{bio} biofilm conductivity, $\text{mS } \mu\text{m}^{-1}$
- z location in biofilm, μm
- τ time conversion = 60 s min^{-1}
- ν volume conversion = $10^{15} \mu\text{m}^3 \text{ dm}^{-3}$
- $\gamma_{e^-/\text{Suc}}$ electron equivalence of sucrose, $\text{mmol-electron mmol-sucrose}^{-1}$
- $\gamma_{e^-/b}$ electron equivalence of active biomass, $\text{mmol-electron mg-VS}^{-1}$ (assuming $\text{C}_5\text{H}_7\text{O}_2\text{N}$ for VS [5])

The local voltage in the biofilm was related to the local potential and described by the following equation [5]. The local voltage at the biofilm/anode interface would be the anode voltage E_{ano} .

$$E = \eta + E_{K_{\text{ano}}} \quad (9)$$

where

- E local voltage in biofilm, V
- $E_{K_{\text{ano}}}$ Half-max-rate anode voltage, V

The half-max-rate anode voltage was defined as the voltage that occurred when the rate of sucrose consumption was half the maximum rate [5]. The voltage could be described as follows:

$$E_{K_{\text{ano}}} = E_{\text{ano}}^o - \frac{RT}{F} \ln\left(\frac{[\text{EA}]_{\text{ano}}^o}{K_{\text{EA}}}\right) \quad (10)$$

- E_{ano}^o standard anode voltage, V
- $[\text{EA}]_{\text{ano}}^o$ standard anodic concentration of biofilm as electron acceptor = 1 mol dm^{-3}
- K_{EA} half velocity constant for biofilm as electron acceptor, mol dm^{-3}

The open-circuit voltage of the MFC was determined as follows [1]:

$$E_{\text{OC}} = E_{\text{cat}} - E_{\text{ano}} \quad (11)$$

where

- E_{OC} open-circuit voltage of MFC, V

In the biofilm, the concentration of sucrose was a function of both time and location. The mass balance of sucrose, as shown in Eq. 12, complied with both the anodic reaction and the diffusion of sucrose from the bulk liquid through the biofilm. In a similar fashion, the mass balances of hydrogen ion and bicarbonate ion were obtained, as shown in Eqs. 13 and 14, respectively.

$$\frac{\partial}{\partial t} [\text{Suc}]_{\text{bio}} = D_{\text{Suc,bio}} \frac{\partial^2}{\partial z^2} [\text{Suc}]_{\text{bio}} - r_{\text{exo}} \quad (12)$$

Table 1 Parameters in the simulation of the MFC

Symbol	Description	Value	Unit	Reference
α_{cat}	Electron-transfer coefficient of cathode	1.083	Unitless	Calculated [7]
$\gamma_{\text{COD/Suc}}$	COD equivalence of sucrose	384	mg-COD mmol-sucrose ⁻¹	Calculated
$\gamma_{e^-/b}$	Electron equivalence of active biomass	0.177	mmol-electron mg-VS ⁻¹	[5]
$\gamma_{e^-/\text{Suc}}$	Electron equivalence of sucrose	48	mmol-electron mmol-sucrose ⁻¹	Calculated
γ_{e^-/O_2}	Electron equivalence of oxygen	4	mmol-electron mmol-oxygen ⁻¹	Calculated
κ_{bio}	Biofilm conductivity	5×10^{-5}	mS μm^{-1}	[8]
μ_b	Specific growth rate of active biomass	4.792×10^{-4}	min ⁻¹	[8]
ρ_b	Density of active biomass	5×10^4	mg-VS dm ⁻³	[8]
b_{endo}	Endogenous decay coefficient of active biomass	5.556×10^{-5}	min ⁻¹	[8]
$D_{\text{HCO}_3^-, \text{bio}}$	Diffusivity of bicarbonate ion in biofilm	4.96×10^4	$\mu\text{m}^2 \text{min}^{-1}$	[12]
$D_{\text{Suc, bio}}$	Diffusivity of sucrose in biofilm	6.24×10^3	$\mu\text{m}^2 \text{min}^{-1}$	[12]
D_{H^+}	Diffusivity of hydrogen ion in water	5.58×10^5	$\mu\text{m}^2 \text{min}^{-1}$	[13]
$D_{\text{O}_2, \text{PTFE}}$	Diffusivity of oxygen in PTFE	1.01×10^3	$\mu\text{m}^2 \text{min}^{-1}$	[14]
E_{ano}°	Standard anode voltage	0.095	V	Calculated [1, 15]
E_{cat}°	Standard cathode voltage	1.229	V	[1]
F	Faraday's constant	96,485	C mol ⁻¹	[5]
k_{O_2}	Rate constant of oxygen reduction per area	5.48×10^{-6}	mmol dm ⁻² min ⁻¹	Calculated [7]
K_{EA}	Half velocity constant for biofilm as electron acceptor	2.33×10^{-6}	mmol dm ⁻³	Calculated [5, 8]
K_{Suc}	Half velocity constant for sucrose	2.09	mmol dm ⁻³	Assumed [16]
K_{O_2}	Half velocity constant for oxygen	4×10^{-3}	mmol dm ⁻³	[7]
R	Gas constant	8.3145	J mol ⁻¹ K ⁻¹	[5]
X_b	Volume fraction of active biomass	0.5	Unitless	Assumed
Y_b	Active biomass growth yield	0.049	mg-VS mg-COD ⁻¹	[8]

where

$D_{\text{Suc, bio}}$ diffusivity of sucrose in biofilm, $\mu\text{m}^2 \text{min}^{-1}$

$$\frac{\partial}{\partial t} [\text{H}^+]_{\text{bio}} = D_{\text{H}^+} \frac{\partial^2}{\partial z^2} [\text{H}^+]_{\text{bio}} + 60r_{\text{exo}} \quad (13)$$

where

$[\text{H}^+]_{\text{bio}}$ concentration of hydrogen ion in biofilm, mmol dm⁻³

D_{H^+} diffusivity of hydrogen ion in water, $\mu\text{m}^2 \text{min}^{-1}$

$$\frac{\partial}{\partial t} [\text{HCO}_3^-]_{\text{bio}} = D_{\text{HCO}_3^-, \text{bio}} \frac{\partial^2}{\partial z^2} [\text{HCO}_3^-]_{\text{bio}} + 12r_{\text{exo}} \quad (14)$$

where

$[\text{HCO}_3^-]_{\text{bio}}$ concentration of bicarbonate ion in biofilm, mmol dm⁻³

$D_{\text{HCO}_3^-, \text{bio}}$ diffusivity of bicarbonate ion in biofilm, $\mu\text{m}^2 \text{min}^{-1}$

All the parameters applied in the above equations were obtained from various literatures, as shown in Table 1.

Some assumptions were made, since not all aspects of MFC have been thoroughly studied yet.

Numerical approximation

A numerical approximation technique was required to solve the above differential equations. The selected technique was the implicit finite difference method [10]. For instance, Eq. 3 was transformed into the following equation.

$$\frac{[\text{O}_2]_{i,j} - [\text{O}_2]_{i,j-1}}{t_j - t_{j-1}} = D_{\text{O}_2, \text{PTFE}} \left\{ \frac{[\text{O}_2]_{i+1,j} - 2[\text{O}_2]_{i,j} + [\text{O}_2]_{i-1,j}}{(z_i - z_{i-1})^2} \right\} \quad (15)$$

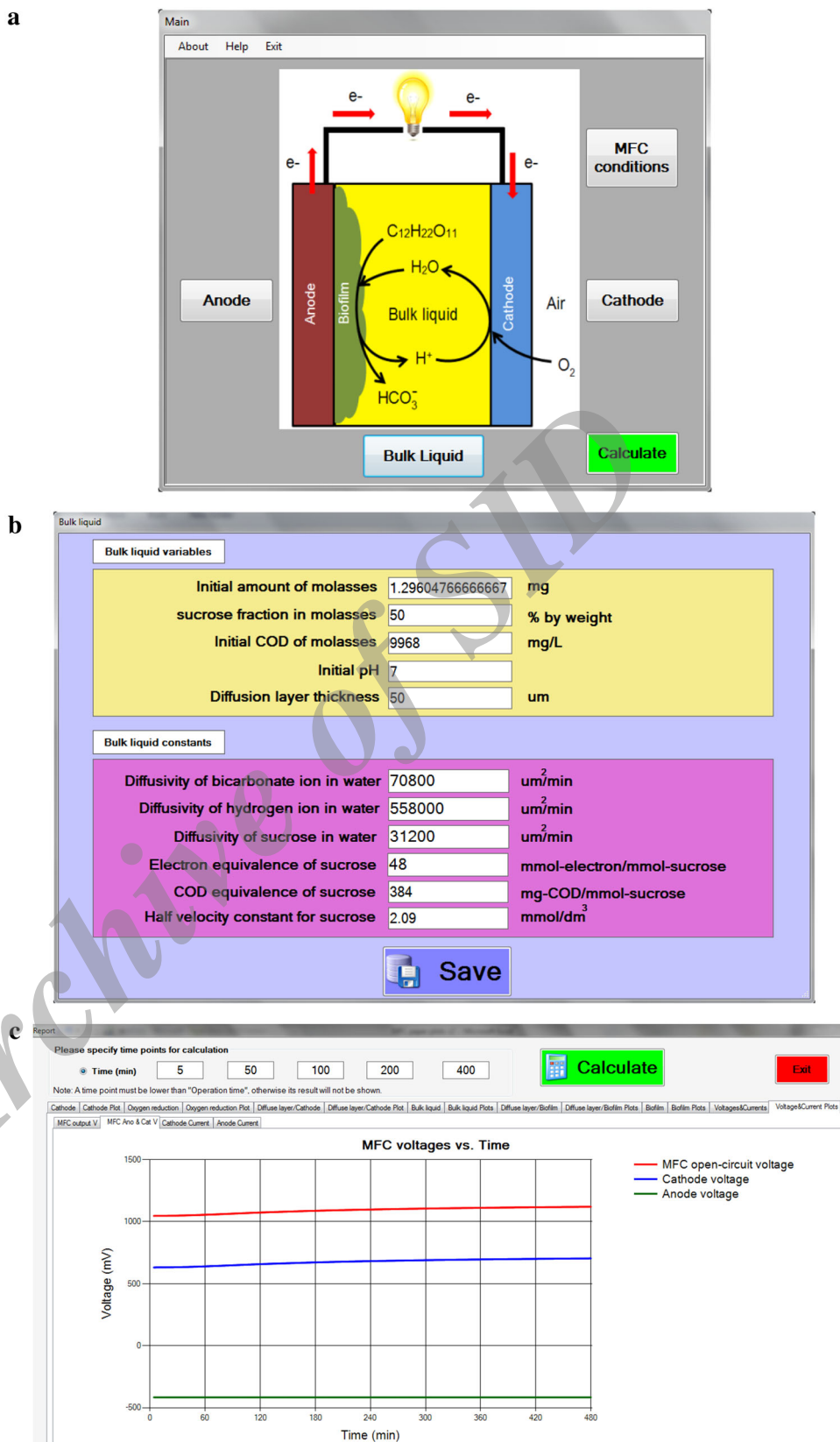
where

i index indicating location i

j index indicating time j

Equation 15 was rewritten into an equation of vectors and matrices that contained the values of the concentration of oxygen at every location in the PTFE layer. For example, if the layer is partitioned to consist of four locations

Fig. 2 Examples of screen captures of the MFC simulation program: the main window (a), the input window of the bulk liquid (b), and the result window (c)



inside, Eq. 15 then becomes the following equation. The subscript t indicates that all the concentrations in the vector are at time t .

$$\frac{1}{\Delta t} \left(\begin{bmatrix} [O_2]_1 \\ [O_2]_2 \\ [O_2]_3 \\ [O_2]_4 \end{bmatrix}_t - \begin{bmatrix} [O_2]_1 \\ [O_2]_2 \\ [O_2]_3 \\ [O_2]_4 \end{bmatrix}_{t-\Delta t} \right) = \frac{D_{O_2,PTFE}}{(\Delta z)^2} \begin{bmatrix} -2 & 1 & 0 & 0 \\ 1 & -2 & 1 & 0 \\ 0 & 1 & -2 & 1 \\ 0 & 0 & 1 & -2 \end{bmatrix} \begin{bmatrix} [O_2]_1 \\ [O_2]_2 \\ [O_2]_3 \\ [O_2]_4 \end{bmatrix}_t - \begin{bmatrix} [O_2]_0 \\ 0 \\ 0 \\ [O_2]_5 \end{bmatrix} \quad (16)$$

where

Δt $t_j - t_{j-1}$ = time interval

Δz $z_i - z_{i-1}$ = distance interval

Equation 16 could be rewritten into an abbreviated general form as follows:

$$\frac{1}{\Delta t} \left(\underline{[O_2]}_t - \underline{[O_2]}_{t-\Delta t} \right) = \frac{D_{O_2,PTFE}}{(\Delta z)^2} \left(\mathbb{A} \underline{[O_2]}_t - \underline{a} \right) \quad (17)$$

Equation 17 was then rearranged into the form of $\mathbb{B}\underline{x} = \underline{b}$. Since the matrix \mathbb{B} was a tridiagonal matrix, an algorithm for solving a tridiagonal system by elimination [17] was applied to solve for the vector \underline{x} , which was $[O_2]$, in this case, as shown in the following equation.

$$\left(\mathbb{I} - \frac{\Delta t D_{O_2,PTFE}}{(\Delta z)^2} \mathbb{A} \right) \underline{[O_2]}_t = \underline{[O_2]}_{t-\Delta t} + \frac{\Delta t D_{O_2,PTFE}}{(\Delta z)^2} \underline{a} \quad (18)$$

where

\mathbb{I} identity matrix

Results and discussion

The MFC simulation program accepted inputs including the initial amount of sucrose, pH, operation time, temperature, and biofilm thickness. The program allowed the user to modify values of some parameters, if more accurate values were acquired. Figure 2 shows some screen captures of the program. The program displayed the results in two formats; tables and plots. The results included, for example, the concentration of sucrose in the bulk liquid, the concentration of oxygen in the PTFE layer, the

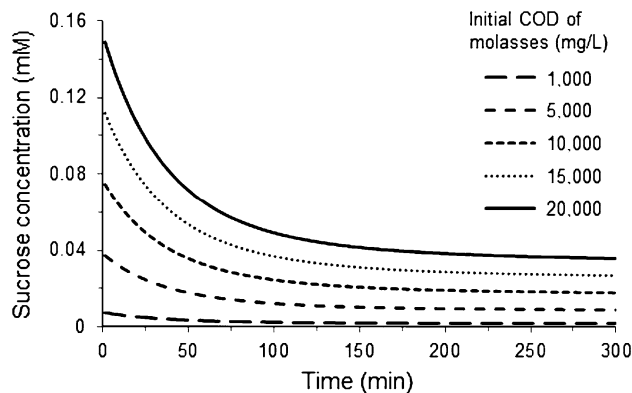


Fig. 3 Plots of sucrose concentration in the bulk liquid over time at different initial concentrations of molasses

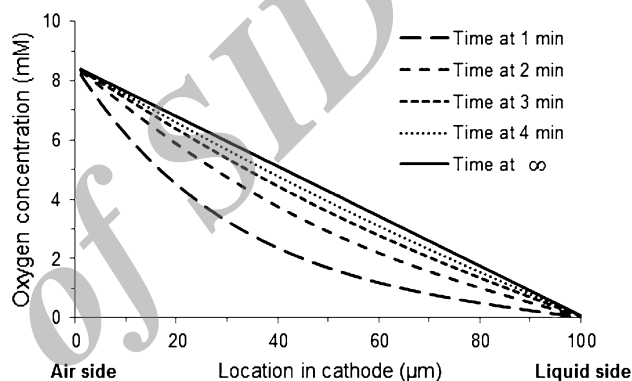


Fig. 4 Plots of oxygen concentration in the PTFE layer (100 μm thick) at different times

concentration of sucrose in the biofilm layer, the cathode and anode voltages, and the MFC open-circuit voltage.

Plots of sucrose concentration in the bulk liquid at various initial levels of chemical oxygen demand (COD) of molasses are shown in Fig. 3. The higher initial COD level of molasses resulted in the higher initial rates of diffusion into the biofilm and bacterial consumption of sucrose. The sucrose concentration quickly decreased in the first 50 min, slowly decreased at later time, and almost became steady eventually.

The concentration profiles of oxygen in the PTFE layer at different times are shown in Fig. 4. Thickness of the layer was assumed to be 100 μm . Oxygen concentration in the air was assumed to be in excess and thus constant. The bulk liquid was depleted of oxygen since it was completely consumed in the reduction reaction. As shown in the plots, the concentration almost quickly reached the linear saturation line in the first few minutes. The oxygen profile in the PTFE layer remained unchanged and unaffected by the changing sucrose concentration throughout the MFC operation.

The concentration profiles of sucrose in the biofilm layer are shown in Fig. 5. The biofilm thickness was assumed to

Fig. 5 Plots of sucrose concentration in the biofilm layer (60 μm thick) at different times. The initial COD level of molasses in the bulk liquid was 10,000 mg/L

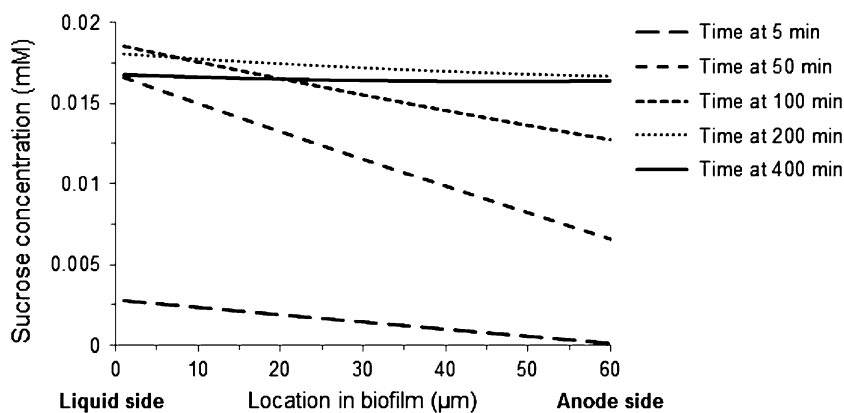
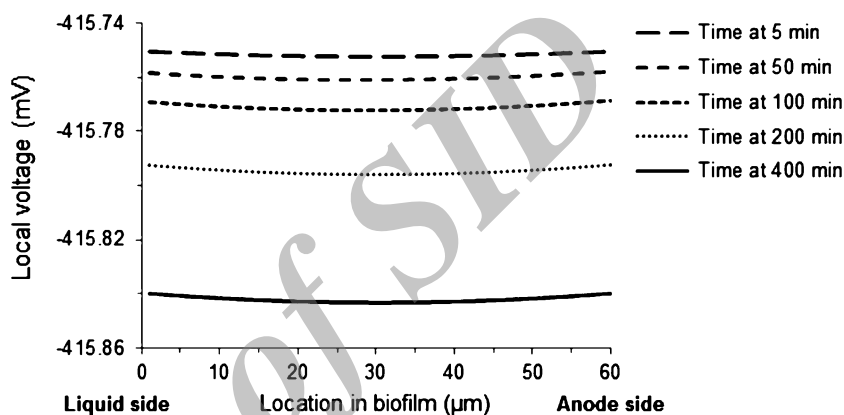


Fig. 6 Plots of local voltage in the biofilm layer (60 μm thick) at different times. The initial COD level of molasses in the bulk liquid was 10,000 mg/L



be 60 μm [18] and the initial COD level of molasses in the bulk liquid to be 10,000 mg/L. The sucrose concentration quickly increased in the early period due to the diffusion of sucrose from the bulk liquid into the biofilm layer. The concentration eventually remained almost constant, since it was not different from the sucrose concentration in the bulk liquid, and thus it reached saturation. The rate of sucrose consumption by the bacteria was not as fast as the diffusion rate of sucrose.

The local voltage profiles in the biofilm layer are shown in Fig. 6. The local voltages gradually decreased, becoming more negative over time, as the rate of electron generation by the respirations increased due to more sucrose molecules diffused into the biofilm. Although the plots did not show it clearly, the voltages close to the anode were slightly higher than those close to the bulk liquid. As a result, the generated electrons flowed toward the anode with the higher voltage, and the electric current flowed in the opposite direction. The local voltage became more negative when increasing the initial COD level of molasses, but the difference in the magnitudes was very small.

The effects of cathode thickness and biofilm thickness on the open-circuit voltage of the MFC are presented by plots in Fig. 7. The voltage values were obtained at 60 min. For the results in Fig. 7a, the biofilm thickness was kept at 60 μm, and the thickness of the PTFE layer was varied

between 50 and 300 μm. As the thickness increased, the concentration of oxygen molecules that diffused through the cathode and participated in the reduction reaction decreased. This led to the lower cathode voltage, and thus the lower open-circuit voltage. The higher COD level of molasses resulted in the higher voltage, since more hydrogen ions were produced from the oxidation of sucrose and participated in the reduction.

For the results in Fig. 7b, thickness of the PTFE layer was kept at 100 μm, and the biofilm thickness was varied between 10 and 260 μm. As the thickness increased, more bacteria were available to oxidize sucrose, which resulted in more produced electrons, the lower anode voltage, and the higher open-circuit voltage. The higher COD level of molasses resulted in the higher voltage, since more sucrose molecules were oxidized. The difference in the biofilm thickness had a greater effect on the voltage at the higher COD levels. Perhaps at the low amount of sucrose molecules, they were mostly consumed by the bacteria near the bulk liquid. As a result, the thicker biofilm with more bacteria did not result in a significant difference. In addition, if the biofilm were too thin, the bacteria in small numbers could not keep up with the high amount of sucrose. The voltage thus hardly increased with the increasing amount of sucrose.

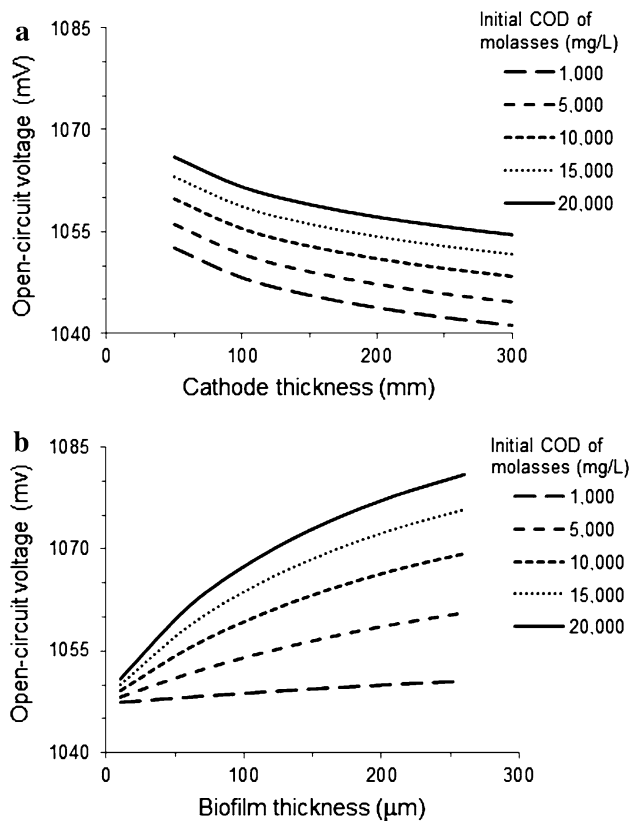


Fig. 7 Plots of the open-circuit voltages as a function of thickness of the PTFE layer (a) and thickness of the biofilm (b) at different initial COD levels of molasses

When comparing between the effects of the PTFE layer and the biofilm on the voltage, at the COD levels $>5,000$ mg/L changing thickness of the biofilm resulted in a more significant effect on the voltage than changing thickness of the PTFE layer. The biofilm involved both the diffusion and bacterial oxidation of sucrose, while the PTFE layer only involved the diffusion of oxygen. The reduction of oxygen should only occur at the cathode/liquid interface.

Sevda et al. [19] studied air-cathode MFCs operating on molasses mixed sewage wastewater. Modeling after the reported MFC, several simulation parameters were adjusted. A few assumptions, however, had to be made, since certain parameters of the MFC system were not reported. With the COD level of $9,968 \pm 32$ mg/L, the reported MFC could yield an open-circuit voltage of 750–771 mV. At the same COD level, these numbers were lower than the voltage estimated by the simulation program, which could only go down to about 1,000 mV. Model validation with more experimental data and more accurate model parameters are needed, before the program can be used in prediction and optimization of the MFC performance in practice. Nevertheless, the simulation results regarding the

kinetics of the MFC seemed to agree with the theories and provided better understanding of the process.

Conclusions

The simulation program was able to compute and provide the concentration profiles of sucrose (the main component of molasses) and an open-circuit voltage of the MFC. As the cathode thickness decreased or the biofilm increased, the voltage increased. The biofilm thickness had a greater effect on the voltage than the cathode thickness when the initial COD levels were $>5,000$ mg/L.

Acknowledgments At the initial stage, the simulation program was partially developed by Napatsanun Wongsamajana and Katanyuta Sirikhum, undergraduate students in the Department of Chemical Engineering, Thammasat University.

Conflict of interest The author declares that he has no competing interests.

Open Access This article is distributed under the terms of the Creative Commons Attribution License which permits any use, distribution, and reproduction in any medium, provided the original author(s) and the source are credited.

References

1. Logan, B.E., Hamelers, B., Rozendal, R., Schröder, U., Keller, J., Freguia, S., Aelterman, P., Verstraete, W., Rabaey, K.: Microbial fuel cells: methodology and technology. *Environ. Sci. Technol.* **40**(17), 5181–5192 (2006). doi:10.1021/es0605016
2. Pant, D., van Bogaert, G., Diels, L., Vanbroekhoven, K.: A review of the substrates used in microbial fuel cells (MFCs) for sustainable energy production. *Bioresour. Technol.* **101**(6), 1533–1543 (2010). doi:10.1016/j.biortech.2009.10.017
3. Liu, H., Logan, B.E.: Electricity generation using an air-cathode single chamber microbial fuel cell in the presence and absence of a proton exchange membrane. *Environ. Sci. Technol.* **38**(14), 4040–4046 (2004). doi:10.1021/es0499344
4. Binkley, W.W., Wolform, M.L.: Composition of cane juice and cane final molasses. In: Claude, S.H., Melville, L.W. (eds.) *Advances in Carbohydrate Chemistry*, vol. 8, pp. 291–314. Academic Press, New York (1953)
5. Kato Marcus, A., Torres, C.I., Rittmann, B.E.: Conduction-based modeling of the biofilm anode of a microbial fuel cell. *Biotechnol. Bioeng.* **98**(6), 1171–1182 (2007). doi:10.1002/bit.21533
6. Picioreanu, C., Head, I.M., Katuri, K.P., van Loosdrecht, M.C.M., Scott, K.: A computational model for biofilm-based microbial fuel cells. *Water Res.* **41**(13), 2921–2940 (2007). doi:10.1016/j.watres.2007.04.009
7. Zeng, Y., Choo, Y.F., Kim, B.-H., Wu, P.: Modelling and simulation of two-chamber microbial fuel cell. *J. Power Sources* **195**(1), 79–89 (2010). doi:10.1016/j.jpowsour.2009.06.101
8. Merkey, B.V., Chopp, D.L.: The performance of a microbial fuel cell depends strongly on anode geometry: a multidimensional modeling study. *Bull. Math. Biol.* **74**(4), 834–857 (2012). doi:10.1007/s11538-011-9690-0
9. Olbrich, H.: *The Molasses*. Biotechnologie-Kempe GmbH (2006), Germany (1963)

10. Zielke, E.A.: Numerical analysis of a one dimensional diffusion equation for a single chamber microbial fuel cell using a linked simulation optimization (LSO) technique. In: E521: Advanced Numerical Methods. (2006)
11. Torres, C.I., Marcus, A.K., Lee, H.-S., Parameswaran, P., Krajmalnik-Brown, R., Rittmann, B.E.: A kinetic perspective on extracellular electron transfer by anode-respiring bacteria. *FEMS Microbiol. Rev.* **34**(1), 3–17 (2010). doi:[10.1111/j.1574-6976.2009.00191.x](https://doi.org/10.1111/j.1574-6976.2009.00191.x)
12. Stewart, P.S.: Diffusion in biofilms. *J. Bacteriol.* **185**(5), 1485–1491 (2003)
13. Torres, C.I., Kato Marcus, A., Rittmann, B.E.: Proton transport inside the biofilm limits electrical current generation by anode-respiring bacteria. *Biotechnol. Bioeng.* **100**(5), 872–881 (2008). doi:[10.1002/bit.21821](https://doi.org/10.1002/bit.21821)
14. Rharbi, Y., Yekta, A., Winnik, M.A.: A method for measuring oxygen diffusion and oxygen permeation in polymer films based on fluorescence quenching. *Anal. Chem.* **71**(22), 5045–5053 (1999). doi:[10.1021/ac990193c](https://doi.org/10.1021/ac990193c)
15. Thauer, R.K., Jungermann, K., Decker, K.: Energy conservation in chemotrophic anaerobic bacteria. *Bacteriol. Rev.* **41**(1), 100–180 (1977)
16. van Niel, E.W.J., Claassen, P.A.M., Stams, A.J.M.: Substrate and product inhibition of hydrogen production by the extreme thermophile *Caldicellulosiruptor saccharolyticus*. *Biotechnol. Bioeng.* **81**(3), 255–262 (2003). doi:[10.1002/bit.10463](https://doi.org/10.1002/bit.10463)
17. Conte, S.D., de Boor, C.: The solution of linear system by elimination. In: Elementary Numerical Analysis: An Algorithmic Approach, pp. 147–157. McGraw-Hill, New York (1980)
18. Lee, H.-S., Torres, C.S.I., Rittmann, B.E.: Effects of substrate diffusion and anode potential on kinetic parameters for anode-respiring bacteria. *Environ. Sci. Technol.* **43**(19), 7571–7577 (2009). doi:[10.1021/es9015519](https://doi.org/10.1021/es9015519)
19. Sevda, S., Dominguez-Benetton, X., Vanbroekhoven, K., De Wever, H., Sreerishnan, T.R., Pant, D.: High strength wastewater treatment accompanied by power generation using air cathode microbial fuel cell. *Appl. Energy* **105**, 194–206 (2013). doi:[10.1016/j.apenergy.2012.12.037](https://doi.org/10.1016/j.apenergy.2012.12.037)

Archive of SID